# Modelling charge transfer processes in $C^{2+}$–tetrahydrofuran collision for ion-induced radiation damage in DNA building blocks

Ewa Erdmann [a] Marie-Christine Bacchus-Montabonel [b] and Marta Łabuda [a]

Investigations of collision-induced processes involving carbon ions and molecules of biological interest, in particular DNA building blocks, are crucial to model the effect of radiation on cells in order to improve medical treatments for cancer therapy. Using carbon ions appears to be one of the most efficient ways to increase biological effectiveness to damage cancerous cells by irradiating deep-seated tumors. Therefore, interest in accurate calculations to understand fundamental processes occurring in ion–molecule collision systems has been growing recently. In this context, the charge transfer process in the collision of $C^{2+}(1s^2 2s^2)$ ions with the heterocyclic sugar moiety building block tetrahydrofuran (THF) was studied in order to interpret the mechanisms occurring at the molecular level. The molecular structure properties of THF were obtained by means of *ab initio* quantum chemistry methods. The role of the conformational structure and the orientation of the THF molecule in collision with $C^{2+}$ ions are particularly discussed. Anisotropic effects of the process dynamics in the collision energy ranging from eV to keV by means of semiclassical treatment are also presented and compared to previous experimental and theoretical investigations. A detailed analysis of the obtained cross sections points out an increase in these values by three orders of magnitude by a change of the THF symmetry from $C_{2v}$ to $C_s$ in collision with $C^{2+}$, which determines a more efficient charge transfer in this case.

DOI: 10.1039/c7cp02100c

## 1. Introduction

An extensive research study has focused on understanding the effects of ionizing radiation on living matter, and an enormous amount of work has been carried out in this field, especially in the past two decades. It has been shown that the interaction of ionizing radiation with biological tissue can induce different types of damage or modifications to DNA. These effects can increase the risk of cancer, but they can also be used in a positive way, as in heavy ion radiotherapy. Most significant biological consequences are related to single- and double-strand breaks caused by radiations with DNA chains. It is known that direct damage to DNA is not only due to the primary quanta of radiation itself, but also to secondary particles generated along the track after the interaction of the ionizing radiation with the biological medium.[1,2] These particles may be either low energy electrons, radicals, or singly and multiply charged ions. A lot of experiments and theoretical studies have been performed recently in order to investigate the action of these particles on biologically relevant molecules.

From the experimental point of view, many studies have thus focused on the dynamics of molecular ionization and fragmentation processes induced by the interaction of photons,[3,4] low-energy electrons[5–8] and keV ions[4,9,10] with biomolecules. They allow an evaluation of the relative cross sections for different reactions directly from the mass spectra. Unfortunately, such experimental results, focused mainly on the fragmentation process, cannot provide any information on possible charge transfer. Obviously, theoretical approaches and simulations help following the main processes which can occur during ion–(bio)molecule collisions. Those can be either: excitation and fragmentation of the biomolecule, ionization of the target and possible electron capture from the biomolecule towards the multicharged ion.

The most recent investigations using different experimental techniques have been devoted to the fragmentation of THF molecules induced by photons,[11,12] low energy electrons[13–17] and neutral potassium atoms.[18,19] However, from the theoretical point of view, less is known about the efficiency and accuracy of quantum chemistry methods for the determination of the structural properties of the THF molecule and the dynamics of the processes in these collisional systems. A precise analysis of the possible channels for charge exchange processes

[a] *Faculty of Applied Physics and Mathematics, Gdańsk University of Technology, Narutowicza 11/12, 80-233 Gdańsk, Poland. E-mail: marta.labuda@pg.gda.pl*

[b] *Univ Lyon, Université Claude Bernard Lyon 1, CNRS, Institut Lumière Matière, F-69622 Villeurbanne, France*

(capture of single and double electrons) requires very accurate potential energy curves and couplings that are usually determined by *ab initio* quantum chemistry approaches. A good assessment of the employed methods is also necessary to calculate with high precision the charge transfer cross sections. The prediction of the order of magnitude of the cross sections provides valuable information concerning the elucidation of the charge exchange and fragmentation mechanisms.

One of the main motivations of our theoretical investigation is the very recent experimental study of the fragmentation processes of THF molecules induced by $C^+$, $H^+$ and $O^+$ collision for incident energies between 25 eV and $\sim$1 keV.[20] Here, using cation-induced luminescence spectroscopy, several neutral fragments, as well as singly ionized C, H and O atoms, were detected and compared with the existing spectroscopic data. Moreover, in this experiment, it has been shown that the fragmentation mechanism strongly depends on the projectile and is dominated by electron transfer from tetrahydrofuran molecules to the projectile cations. For the specific $C^+$–THF collision, it was postulated that the rapid enhancement of the CH ($A^2\Delta$) fragmentation yield, which occurred at lower velocities, may indicate the formation of the temporary $[C–C_4H_8O]^+$ complex prior to dissociation.

Therefore, our theoretical efforts focused on the determination of electron capture cross sections with THF at keV impact energy as in the collisions of heavy ions with nucleobases.[21–24] In particular, the inclusion of carbon ions is proven to be the best choice for selectively irradiating deep-seated tumors during therapy. For such systems, we have thus proposed and developed a uniform framework based on the *ab initio* molecular calculations of the potentials and nonadiabatic couplings between the different molecular states involved in the process followed by collisional dynamics in a wide energy range of interactions, from eV to keV. Our first prototypical study of the charge transfer process for the $C^{q+}$ + uracil system for a series of charge $q$ = [2–4] has shown that the fragmentation and charge exchange process appear to be complementary.[21] Indeed, this was in agreement with the experimental data in which the relative uracil fragmentation cross sections for the interaction with $C^{q+}$ have been measured. A general conclusion from the experimental findings was that the relative fragmentation yield for a molecular target after impact with a projectile ion can be assumed to be inversely proportional to the electron capture cross section.[9] The effects of the projectile electronic structure have also been discussed. The details of the model will be discussed in the following sections.

Consequently, in recent calculations we have selected five- and six-membered heterocyclic molecules, which can also serve as simple models of the DNA structural units (nucleic bases, deoxyribose) in the investigations of the action of ionizing radiation in biologically important materials, as well as in the synthesis of new compounds which are especially useful in medicinal chemistry. The tetrahydrofuran ($C_4H_8O$) (Fig. 1a) molecule has attracted a lot of attention owing to its applications in many chemical areas. It is regarded as the simplest analogue of the 2-deoxy-D-ribose (dR) ($C_5H_{10}O_4$) and D-ribose ($C_5H_{10}O_5$) molecules, which are one of the most important molecules in DNA and RNA structures. Deoxyribose plays a crucial role as a linker between the phosphate groups and nucleobases in the DNA chain and it can occur in its furanose or pyranose form depending on the environment. This simple THF heterocyclic five-membered molecule has been extensively studied in the past with respect to both its vibrational and electronic structure by experimental[13–15,17,25–27] and theoretical approaches.[28–32] Many studies have focused on the pseudorotational properties of tetrahydrofuran, but the geometry of the equilibrium structures still remain unclear. According to recent investigations,[14] the most stable THF structure is a $C_S$-symmetric envelope conformation.

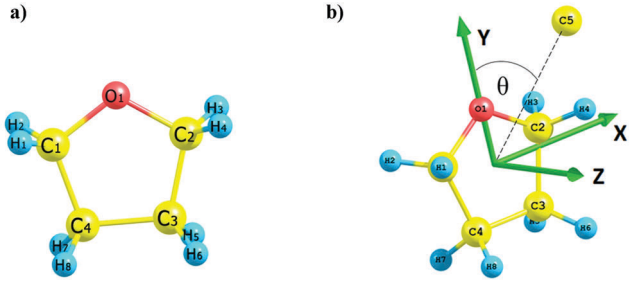


Fig. 1 (a) Internal coordinates and numbering of the atoms in THF and (b) molecular model of the collision: planar for $\theta = 0^\circ$ and perpendicular for $\theta = 90^\circ$.

Here, in order to understand the charge transfer mechanism we introduce the results of the latest investigations of the collision of $C^{2+}(1s^22s^2)$ ions with the THF heterocyclic molecule.[20,33] No detailed theoretical study of the potential energy curves and nonadiabatic couplings, which are important for an evaluation of the charge transfer cross sections, is reported in the literature for this system. Therefore, as a first step, we carefully analyzed the charge transfer for this $C^{2+}$–THF reaction, including different orientations of the target molecule investigated, for the simplicity of calculations in two chosen conformers: envelope with $C_s$ symmetry and planar with $C_{2v}$ symmetry. Particularly, dependence of the geometry on the molecular target was observed in the fragmentation process, pointing out different fragmentation pathways with regard to the conformation of the molecular target.[34] We plan to investigate the dependence of the charge transfer dynamics not only on the collision energy but also on the orientation of the target molecule during the collision as well as on the electronic structure of the ionized projectile. In order to obtain an intrinsic picture of the dynamics of the process, the obtained results were compared with those performed on 2-deoxy-D-ribose with $C^{4+}$ ions.[35,36] The present article is organized as follows: Section 2 presents the collisional model and the computational methods employed to calculate potential energy curves, couplings and charge transfer cross sections. The obtained results are given and discussed in detail in Section 3. Finally, in Section 4, conclusion remarks and perspectives are included.

## 2. Theoretical treatment

### 2.1. Molecular model

A complete study of the mechanism and quantitative characteristics of charge exchange processes in the $C^{2+}$–THF interaction

requires a model that is simple enough to be computationally feasible, but which includes sufficient details of the problem to reproduce the essential features of the process. In a theoretical treatment of such a system, as a first step we have to determine the structure of the THF molecule as well as the potential energies and couplings of the different molecular states involved in the collision process. In general, the molecular system is complex, and a complete treatment should take into account all the possible vibration and rotation movements, which of course would lead to a number of degrees of freedom impossible to handle in a calculation. In 2005, we showed it was possible to extend the close-coupling method, which is well-adapted to the treatment of charge transfer processes in ion-atom collisions,[37–39] to much more complex systems, in particular those of biological interest. As a first case study we choose the $C^{q+}$ ($q$ = 2–4)–uracil system.[21] A simple model of this polyatomic complex collisional system was proposed by means of the one-dimensional reaction coordinate approximation in which a projectile ion approaches the corresponding target molecule on a single straight-line trajectory. Under such an assumption, in the case of an interaction of the THF molecule with carbon ions, the collision can be represented as the evolution of the polyatomic $C^{2+}$–THF complex, which, in a first approximation, could be treated as a pseudo-diatomic system, the reaction coordinate corresponding to the distance $R$ between the center-of-mass of the THF molecule and the colliding carbon ion. Since the charge transfer process is extremely fast, the geometry of the THF target can be considered as frozen during the collision time. Of course, such an approach does not consider the degrees of freedom of the complex and the internal motions of the molecule, but seems reasonable in a very fast collision process where nuclear vibration and rotation periods are assumed to be much longer than the collision time (typically $10^{-16}$ s).

For the heterocyclic THF molecule, the geometry is constructed around a five-membered planar ($C_{2v}$ symmetry) ring, and the anisotropy of the charge transfer process can be considered for different orientations of the projectile ion toward this ring plane, for the collision of $C^{2+}$–THF. In such a case, different molecular states of the $C^{2+}$–THF collisional system are involved and the potentials can be calculated along the reaction coordinate $R$ for different angles $\theta$ from perpendicular ($\theta$ = 90°) to planar geometry ($\theta$ = 0°) in order to take into account the anisotropy of the process. The model of the collision is illustrated in Fig. 1b. Additionally, to include a change of the conformation of the target molecule, the collision model also considers the THF molecule in the $C_s$ symmetry (envelope conformer). In such a case, an oxygen atom is displaced by about $\alpha$ = 23.34° from the plane of the THF and the carbon ion approaches along the side of the axis, which is determined within the C–O bond (Fig. 2).

The charge transfer process is mainly driven by the nonadiabatic interactions in the region of the avoided crossings. The corresponding nonadiabatic radial coupling matrix elements between all pairs of states of the same symmetry have

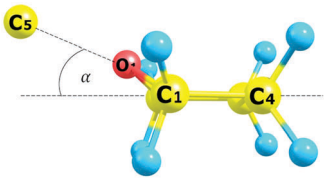


Fig. 2 Geometry of THF in an orientation close to the planar attack. The THF ring is kept in the $C_s$ symmetry; the $\alpha$ angle is a displacement of the oxygen atom (O) from the plane of symmetry of the THF molecule.

been calculated numerically by means of the finite difference technique:

$$g_{KL}^{rad}(R) = \left\langle \Psi_K \left| \frac{\partial}{\partial R} \right| \Psi_L \right\rangle = \lim_{\Delta \to 0} \frac{1}{\Delta} \langle \Psi_K(R) | \Psi_L(R+\Delta) - \Psi_L(R) \rangle$$

$$= \lim_{\Delta \to 0} \frac{1}{\Delta} [\langle \Psi_K(R) | \Psi_L(R+\Delta) \rangle - \langle \Psi_K(R) | \Psi_L(R) \rangle],$$

where $\langle \Psi_K|$ and $|\Psi_L\rangle$ are the eigenfunctions of the different molecular states involved in the process. As $\langle \Psi_K|$ and $|\Psi_L\rangle$ are orthonormal, the expression reduces to $g_{KL}^{rad}(R) = \lim_{\Delta \to 0} \frac{1}{\Delta} \langle \Psi_K(R) | \Psi_L(R+\Delta) \rangle$. The use of this numerical method requires the stability to be checked with respect to the differentiation step $\Delta$. In order to obtain better numerical accuracy, the two-point numerical differentiation method has been used for numerical accuracy with a value of $\Delta$ = 0.0012 a.u. and with the center-of-mass of the THF molecular target chosen as the origin of the coordinates.

### 2.2. Collision dynamics

The collision dynamics of the charge transfer process have been treated by means of the semiclassical method in the framework of the sudden approximation hypothesis. Since electronic transitions are much faster than typical vibration ($\sim 10^{-12}$ s) and rotation motions in the molecule, the molecular target internal degrees of freedom in both the $C_{2v}$ and $C_s$ geometries can be considered to be unchanged during the collision time within the investigated energy range. The absolute total and partial cross sections, corresponding to purely electronic transitions, are then calculated by solving the impact-parameter equation as in the usual ion-atom approach,[40] assuming the geometry of the molecular target fixed in its ground state. In a straight-line impact-parameter treatment, the total electronic wave function is expanded onto a set of configurations built with the product of one-electron orbitals, which are exact solutions of one-electronic two-center Hamiltonian. The introduction of this expansion in the Schrödinger equation leads to a set of coupled equations that is numerically integrated.

Such approximation gives a visual description of what is happening during the collision as it is much easier to picture a classical trajectory than a vector of rapidly oscillating wave functions. In semiclassical approximation, the system follows time evolution as it is very characteristic of classical description. In the impact parameter method, the nuclear trajectory (relative motion of atoms and molecules) is given *a priori* as a

function of time and is treated as a kind of external parameter for the electronic degrees of freedom.

This methodology has been proved to provide quite accurate results for ion-diatomics[38,41] collisions, as well as in ion-polyatomic processes[39] for energies higher than around 10 eV amu$^{-1}$. Effectively, at these collision energies, as previously pointed out for collisions of carbon ions with uracil and halouracils,[21,24,42] the collision time is shown to be much shorter than the typical vibration time and typical rotation time. The present treatment has been extended to collision energies in the eV domain taking into account a recent comparative study of time-dependent quantum wave packet and semiclassical methods in ion-atom charge transfer processes at very low (much below 1 keV)[43–45] and even at ultra low (below 10 eV) energies.[46,47] Nevertheless, the application of quantal wave packet approaches for studying the charge exchange processes with good accuracy is numerically very demanding, as was shown for chosen ion-atom cases,[43,46] especially in a two-dimensional model.[47] Thus, one can always keep in mind a compromise regarding the efficiency and computational cost of the performed calculations. However, the comparative results presented in the literature for the few already investigated cases[44,47,48] lead to the observation that the discrepancy of the quantal approach with respect to the semiclassical approach appears only for the energy of few eV. Therefore, employing semiclassical treatment for ion–(bio)molecule collisions seems to be reasonable as a first choice for understanding the dynamics of the charge exchange process. Particularly, based on our previous experience with the consideration of biological targets, we can thus expect a semiclassical approach to provide a correct order of magnitude of the charge transfer cross sections in a wide collision energy range.

In the present paper, the ion–molecule collision dynamics calculations have been performed in a laboratory energy range from 14.7 eV to 12 keV for both in-the-plane and perpendicular orientations of the $C^{2+}$–THF system. In this energy domain, semiclassical approaches using the EIKONXS code based on an efficient propagation method[49] have been used with good accuracy for impact parameters between 1.5 and 18.5 a.u. All the transitions between the states of the same symmetry, driven by radial coupling matrix elements, have been considered for the colliding $C^{2+}$ carbon ions. The coupled equations have been solved with a step size such that a numerical accuracy of $10^{-4}$ for the symmetry of the $S$ matrix is fulfilled. As previously stated,[21] rotational couplings have not been taken into account in this calculation. To our knowledge, this is the first attempt to generate single and double electron capture cross sections for the collision of the tetrahydrofuran molecule with carbon ions in the considered energy range.

# 3. Results and discussion

## 3.1. Molecular calculations

From a theoretical point of view, we have performed a series of careful quantum chemical calculations of THF. The geometries have been optimized at the Hartree–Fock level as well as at higher *ab initio* levels such as Coupled Cluster Singles Doubles (with parametrical Triples) (CCSD(T)), second order Møller–Plesset (MP2) and by means of Density Functional Theory (DFT) with standard Pople's and Dunning's basis sets. The obtained energy values are presented in Table S1 in the ESI.† Our calculations are in good agreement with other proposed models, which studied pseudo-rotation motion in THF.[29,31] All calculations have been performed by means of the MOLPRO suite of *ab initio* programs.[50,51]

The geometry of the ground state, as well as singly ionized THF molecules, has been optimized by means of DFT calculations using the Becke–Lee–Yang–Parr density functional[52–54] (B3LYP), which has been shown to be computationally efficient and provides accurate structures and transition energies. Geometric parameters (bond lengths and bond angles) for studied conformations of tetrahydrofuran optimized at the B3LYP/6-311++G(d,p) level of theory chosen for further calculations are given in Table S2 in the ESI.† In addition, to specify the order of electronic transitions, the excitation energies, oscillator strengths ($f_L$, in the length gauge) and electronic radial spatial extents ($\langle r^2 \rangle$) of THF were calculated for singlet states with the equation of motion coupled cluster method restricted to single and double excitations (EOM-CCSD)[55] using the geometry previously optimized with B3LYP/6-311G++(d,p). The calculated properties for ten states are presented in Table S3 (for $C_{2v}$ symmetry) and Table S4 (for $C_s$ symmetry) in the ESI.†

In order to determine the potential energy surfaces and couplings of different molecular states involved in the collision process as a function of the internuclear distance $R$, necessary calculations have been carried out at the Complete Active Space Self Consistent Field (CASSCF)[56] level of theory with the chosen 6-311++G(d,p) basis set. Each active space takes into account important orbitals of the THF and carbon ion. Several, carefully chosen active spaces have been considered and will be described in detail for each collision set up. The potential energy curves of the different molecular states involved in the process are determined along the reaction coordinate $R$ for a large number of $R$ values from 0.5 to 10 a.u. Tetrahydrofuran targets in chosen symmetries are considered in their ground state geometry and kept frozen during the collision process.

## 3.2. Potential energy curves

In order to take into account the inner excitations of the electrons in the 5-membered ring in the two different symmetries ($C_{2v}$ and $C_s$) and to analyze their overall influence on the charge transfer process, different active spaces have been constructed and applied in the following calculations. The first considered active space includes the six electrons distributed over three valence and three virtual orbitals, CAS(6,6), constructed mainly on the highest occupied molecular orbital (HOMO) $n_O(2p_z)$ orbital and $2p_y$ orbital centered on an oxygen O atom, as well as the C3–C4 ($2p_z$) orbital of the THF ring. Additionally, the $2p_x$ lowest unoccupied molecular orbital (LUMO), $2p_y$ and $2p_z$ orbitals of the colliding carbon ion are also included. In order to take into account the inner shell molecular orbitals, the active space has been extended to the CAS(10,8), including the doubly occupied

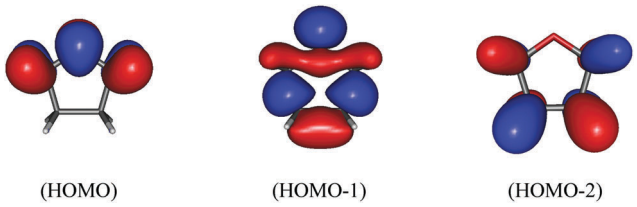


Fig. 3 Main molecular orbitals involved in the charge transfer process located on the THF ($C_{2v}$) ring molecule taken into the active spaces CAS(6,6). The orbital HOMO is defined as $n_O(2p_z^O)$, HOMO−1 as $n_O(2p_y^O)$, and HOMO−2 as $\pi_{C3C4}(2p_z)$.

C3–C4 ($2p_x$) and C3–C4 ($2p_y$) orbitals. The 1s orbitals of all the atoms are treated as frozen cores. The main orbitals of THF in $C_{2v}$ symmetry are presented in Fig. 3.

The corresponding adiabatic potential energy curves for CAS(6,6) in in-the-plane and perpendicular attacks are presented in Fig. 4. Looking carefully at the evolution of the wave function with the internuclear distance $R$ between the colliding $C^{2+}$ ion and the oxygen atom in-the-plane symmetry (Fig. 4a), there is globally no evidence for the presence of a strong avoided crossing, except between states $4^1A_1$ and $5^1A_1$ around $R$ = 2 a.u. Besides, a smooth avoided crossing could be pointed out between states $2^1A_1$ and $3^1A_1$ around $R$ = 3 a.u., but the potential energy curves mainly correspond to their molecular configuration in the asymptotic region. Such an observation was also supported by the determination of the nonadiabatic couplings, where the values obtained were very small (in the order of magnitude between $10^{-8}$ a.u. and $10^{-15}$ a.u., so one can say they were almost negligible). As a consequence, we can expect that for the in-the-plane collisional $C^{2+}$–THF ($C_{2v}$) system, the chosen active space was not sufficient to describe properly the charge transfer process and, consequently, the cross sections could give marginal values in the dynamics calculations. Therefore, as a next step, the collisional system of $C^{2+}$–THF ($C_{2v}$) in the perpendicular direction was investigated for the same active space. For this perpendicular collision, the colliding ion approaches along the $z$ axis and the THF molecule remains in the $xy$ plane with the origin of coordinates at the center-of-mass. Such collisional system presents the $C_s$ symmetry with only A′ and A″ states.

A particularly strong delocalization of the electrons of the target towards the projectile at a close range of internuclear distance $R$ can be seen directly, and an interesting conclusion can therefore be made. Indeed, at first sight, single and double electron captures are clearly observed. The charge transfer process is mainly driven by the nonadiabatic interactions in the vicinity of the avoided crossings. In the perpendicular geometry (Fig. 4b), two significant avoided crossing regions are exhibited around [1.5–1.7] Å between the molecular states $2^1A'$ $\{n_O(2p_z^O)\ 2p_z^C\}$ and $3^1A'$ $\{n_O(2p_y^O)\ 2p_y^C\}$, corresponding to the single electron capture channels with the $C^+ + THF^+$ configuration, as well as between the $5^1A'$ $\{n_O(2p_z^O)\ 2p_y^C 2p_x^C\}$ and $6^1A'$ $\{n_O(2p_z^O)\ 2p_z^C 2p_x^C\}$ where the double electron transfer is observed, leading to the $C + THF^{2+}$ configuration. However, the main process is double excitation of one electron from the $n_O(2p_z^O)$ orbital and one from the $\pi_{C3C4}(2p_z)$ orbital, both of which are located on the

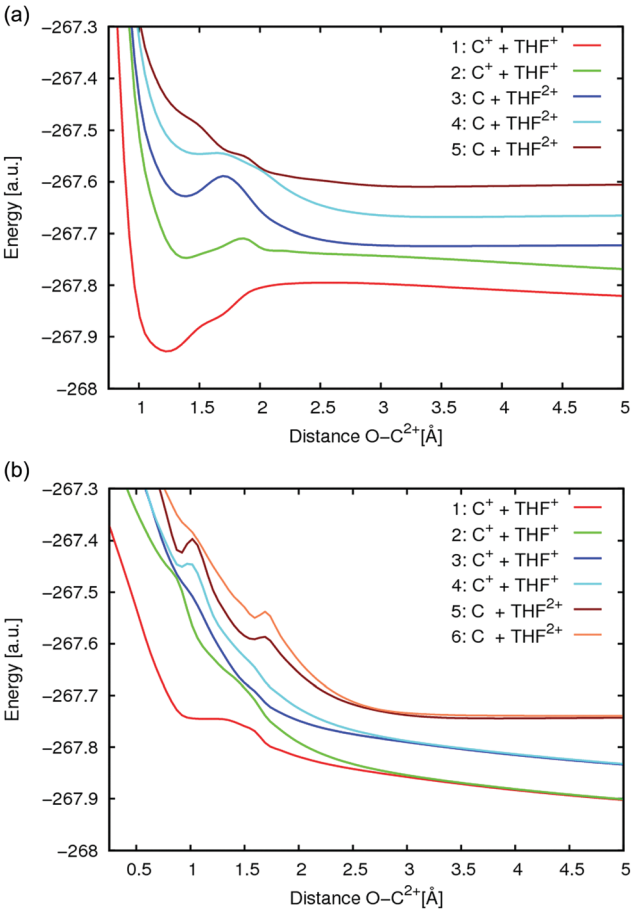


Fig. 4 (a) Adiabatic potential energy curves of the $^1A_1$ states of the $C^{2+}$–THF collision system ($C_{2v}$) in-the-plane orientation along the $y$ axis. Numbering by increasing energy: 1 (red) corresponding to the configuration $\{n_O(2p_z^O)\ 2p_z^C\}$; 2 (green) corresponding to $\{n_O(2p_y^O)\ 2p_y^C\}$; 3 (blue) corresponding to $\{n_O(2p_z^O)\ 2p_y^C\}$ and to $\{\pi_{C3C4}(2p_z)\ 2p_x^C\}$; 4 (light blue) corresponding to $\{n_O(2p_z^O)\ 2p_x^C\}$ and to $\{\pi_{C3C4}(2p_z)\ 2p_y^C\}$; and 5 (brown) corresponding to $\{n_O(2p_y^O)\ 2p_x^C\}$; the second electron capture comes from the $\pi_{C3C4}(2p_z)$ orbital located on the THF ring to $2p_z^C$. (b) Adiabatic potential energy curves of the $^1A'$ states of the $C^{2+}$–THF collision system ($C_{2v}$) in the perpendicular orientation along the $z$ axis. Numbering by increasing energy: 1 (red) corresponding to the configuration $\{n_O(2p_z^O)\ 2p_y^C\}$; 2 (green) corresponding to $\{n_O(2p_z^O)\ 2p_z^C\}$; 3 (blue) corresponding to $\{n_O(2p_y^O)\ 2p_y^C\}$, 4 (light blue) corresponding to $\{n_O(2p_y^O)\ 2p_z^C\}$; 5 (brown) corresponding to $\{n_O(2p_z^O)\ 2p_y^C 2p_x^C\}$; the second electron capture comes from the $\pi_{C3C4}(2p_z)$ orbital located on the THF ring; and 6 (orange) corresponding to $\{n_O(2p_z^O)\ 2p_z^C 2p_x^C\}$; the second electron capture comes from the $\pi_{C3C4}(2p_z)$ orbital located on the THF ring.

THF ring to the 2p components of the colliding carbon, corresponding to the $C + THF^{2+}$ level. The strong degeneration of all the considered states may be observed at the asymptotic region corresponding mainly to the three charge transfer configurations (Fig. 4b): $\{n_O(2p_z^O)\ 2p^C\}$ for states $1^1A'$ and $2^1A'$; $\{n_O(2p_y^O)\ 2p^C\}$ for states $3^1A'$ and $4^1A'$; and $\{n_O(2p_z^O)\ 2p^{2C}\}$ for states $5^1A'$ and $6^1A'$, respectively.

To conclude, we can point out that for the limited active space used in the above calculations the charge transfer appears to be strongly dependent on the orientation of the projectile. For the purpose of extending our approach by including two more inner

shell orbitals, the calculation in-the-plane direction along the $y$ axis for CAS(10,8) has also been performed. The corresponding adiabatic potential energy curves are presented in Fig. 5.

In this case, the calculated five potentials show very interesting features. Firstly, the charge transfer levels present clearly an avoided crossing around $R$ = 2.2 Å between the single capture levels: $2^1A_1$ corresponding to $\{n_O(2p_y^O)\ 2p_y^C\}$ and $3^1A_1$ corresponding to $\{\pi_{C3C4}(2p_x)\ 2p_y^C\}$ configurations, respectively. This is also confirmed in the nonadiabatic coupling calculations (reaching values of $10^{-2}$ a.u.), where the avoided crossing region is favoured for the transition of the electrons. A single electron capture thus takes place mostly from a π-electron of the highest occupied molecular orbital of the THF molecule, $n_O(2p_z^O)$, to the unoccupied 2p orbital of the projectile carbon ion (Fig. 5: states $1^1A_1$ and $2^1A_1$, respectively). This can be attributed to the $\{C^+(1s^22s^22p) + THF^+\}$ level. Additionally, at increasing energy, two simultaneous excitations from the $\pi_{C3C4}(2p_x)$ and $\pi_{C3C4}(2p_y)$ orbitals to the components of the 2p orbital of the colliding carbon ion were found (Fig. 5: $3^1A_1$ and $4^1A_1$) leading to two excited $\{C^+(1s^22s^22p) + THF^{+*}\}$ levels. Effectively, these two levels are correlated adequately with the $2p_y$ and $2p_x$ components of the 2p level of the carbon projectile and evidently they are degenerated at a long range. Such a situation can be noticed by observation of the localization of the electrons at a long range on the active orbitals involved in the reaction. Furthermore, double excitation from the $n_O(2p_z^O)$ and $\pi_{C3C4}(2p_z)$ orbitals on the THF ring to the $2p_y$ and $2p_x$ components of the 2p orbital centered on the colliding carbon ion was also observed, which can be attributed to the $\{C(1s^22s^22p^2) + THF^{2+}\}$ state.

Finally, the molecular calculations for the collision of carbon $C^{2+}$ ions with the THF molecule, being in the $C_s$ symmetry, have been performed. In this case, the collision takes place along the C–O chemical bond corresponding to the $y$ axis and the oxygen atom is slightly displaced from the plane symmetry of the THF molecule by an angle of $\alpha = 23.34°$. To overcome the difficulties concerning the symmetry, the system has been studied using the Cartesian coordinates with the origin at the center-of-mass of the THF molecule. All calculations have been performed with an active space CAS(10,8) taking into account the highest occupied orbitals on the THF ring as well as the $2p_x$, $2p_y$ and $2p_z$ orbitals of the colliding carbon ion. The corresponding potential energy curves in this orientation are presented in Fig. 6. The molecular orbitals of the THF ring involved in the charge transfer are quite similar to those for $C_{2v}$ symmetry. The lowest electronic transitions from the main orbitals of THF in $C_s$ symmetry are given in Table S4 (ESI†).

Looking in detail at the potential energy curves, the trend of the curves radically changes with a decrease in the distance $R$ between the colliding $C^{2+}$ ion and the THF molecule in $C_s$ symmetry. This can be caused by the strong delocalization of the electrons along the C–O bond, especially in the short-range region in which the target and the projectile start to interact. Indeed, two avoided crossings can be observed, one at a distance of around $R$ = 1.7 Å and a second one around $R$ = 2.2 Å, showing strong nonadiabatic interactions between corresponding states (Fig. 6). A very substantial interaction can also be directly noticed between the $\{n_O(2p_z^O)\ 2p_y^C\}$ and $\{n_O(2p_y^O)\ 2p_z^C\}$ levels (Fig. 6: states $2^1A'$ and $3^1A'$, respectively). From the detailed analysis of the calculated results, it can be concluded that both curves do not overlap but show very smooth avoided crossing. However, we think that this feature may be caused by the orientation of the THF target molecule, which has changed with respect to the previous calculations, driving enhanced delocalization of the electrons mainly located on the displaced out-of-plane oxygen atom, especially towards an incoming projectile carbon ion. This could suggest that the charge transfer process may be favorable in the collision system in which the tetrahydrofuran is in the $C_s$ envelope symmetry. Furthermore, in such

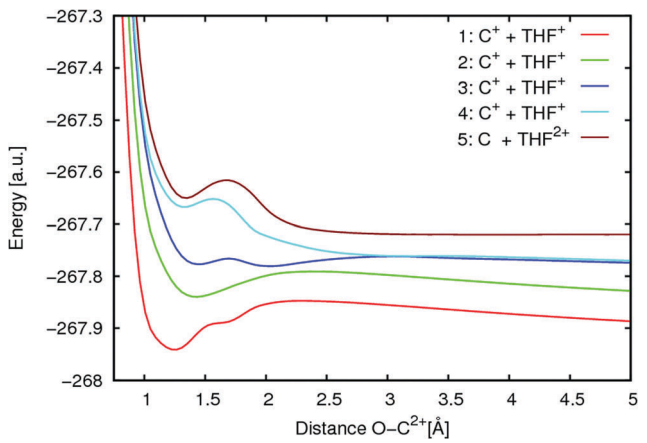


Fig. 5 Adiabatic potential energy curves of the $^1A_1$ states in the collision of $C^{2+}$ ions with THF ($C_{2v}$) in-the-plane orientation along the $y$ axis for CAS(10,8). Numbering by increasing energy: 1 (red) corresponding to the configuration $\{n_O(2p_z^O)\ 2p_z^C\}$; 2 (green) corresponding to $\{n_O(2p_y^O)\ 2p_y^C\}$; 3 (blue) corresponding to $\{\pi_{C3C4}(2p_x)\ 2p_y^C\}$, 4 (light blue) corresponding to $\{\pi_{C3C4}(2p_y)\ 2p_x^C\}$; and 5 (brown) corresponding to $\{n_O(2p_z^O)\ 2p_x^C 2p_y^C\}$; the second electron capture comes from the $\pi_{C3C4}(2p_z)$ orbital located on the THF ring with $\{\pi_{C3C4}(2p_z)\ 2p_x^C 2p_y^C\}$ configuration.

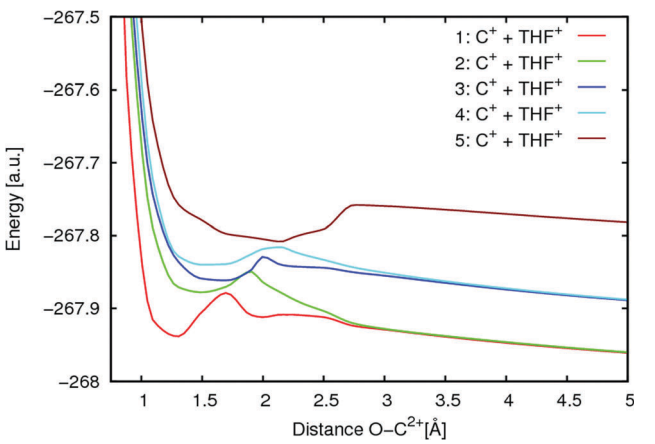


Fig. 6 Adiabatic potential energy curves of the $^1A'$ states in the collision of $C^{2+}$ ions with THF ($C_s$) along the y axis for CAS(10,8). Numbering by increasing energy: 1 (red) corresponding to the configuration $\{n_O(2p_z^O)\ 2p_z^C\}$; 2 (green) corresponding to $\{n_O(2p_z^O)\ 2p_y^C\}$; 3 (blue) corresponding to $\{n_O(2p_y^O)\ 2p_z^C\}$, 4 (light blue) corresponding to $\{n_O(2p_y^O)\ 2p_y^C\}$; 5 (brown) corresponding to $\{\pi_{C3C4}(2p_z)\ 2p_x^C\}$.

a short distance range, one can expect the formation of a temporary cluster molecule leading to the $\{C^+(1s^22s^22p) + THF^+\}$ level.

Moreover, in this case, the process is driven by excitation of the single occupied $n_O(2p^O)$ level centered mainly on the $2p_z$ on the oxygen of the ring to the $2p_z$ and $2p_y$ orbitals of the colliding carbon (Fig. 6: states $1^1A'$ and $2^1A'$, respectively). Both considered states are degenerated at long range and correspond to the $\{C^+(1s^22s^22p) + THF^+\}$ level. Accordingly, for states $3^1A'$ and $4^1A'$, single electron capture takes place from the $n_O(2p^O)$ level centered on the $2p_y$ on the oxygen of the ring to the $2p_z$ and $2p_y$ of the colliding carbon and the highest calculated state corresponds to the excitation of the $n_O(2p^O)$ orbital located on the THF ring toward $2p_x$ of the colliding carbon. No double electron capture has been observed in this case.

In summary, good overall agreement is seen for all the configurations of the molecular system. Indeed, with the change of the orientation of the target molecule from planar or quasi-planar geometry (THF in $C_s$ symmetry with a deviated oxygen atom) to the perpendicular one, interesting features may be observed in the $C^{2+}$–THF collision system. In each considered case, regardless of the orientation of the molecular system, single and/or double electron captures have been observed, taking place from the valence orbitals of the THF molecule to the 2p orbital of the colliding carbon ion $C^{2+}$. This suggests, in agreement with previous experimental observations on ion–molecule collisional systems,[57–59] that in such processes we can expect a strong electronic rearrangement with predominance of multielectron capture from the electronic cloud of the THF molecule towards the $C^{2+}$ colliding ion. Additionally, the same features may be observed in the perpendicular and close to the planar geometry of the system in which in both cases we observed strong degeneration of the single electron transfer levels and, in the case of perpendicular attack for $\theta = 90^\circ$, double electron transfer.

It is worth pointing out that the position of the avoided crossings, as well as the delocalization of the electrons from the target molecule to the projectile, are strongly dependent on the orientation of the collision system. Generally, it seems that the interaction between colliding species occurs much more smoothly at lower internuclear distances when the approach angle decreases and moves from perpendicular geometry to a geometry closer to the planar one. At the lower angle, as for example a displacement $\alpha = 23.34^\circ$ of the oxygen atom out-of-plane of the $C_4H_8O$ molecule, the molecular system is dominated by short range avoided crossings between different potentials. Additionally, in the avoided crossing region for low values of $R$, where the transfer can occur, we could also observe step by step formation of the chemical bonding between the oxygen atom of the THF and the projectile carbon, indicating the possibility for the formation of the molecular complex $[C^+–C_4H_8O]^+$ prior to dissociation.

Indeed, such a result is in agreement with the experimental fragmentation studies induced by the $C^+$–THF collision in which the existence of the $[C–C_4H_8O]^+$ complex has been determined. In this case, investigation of the highest yields obtained for the production of excited C atoms in the $C^+$–THF collision suggested that the fragmentation processes are mostly preceded by electron transfer from the THF molecule to the cation[20] in agreement with the previous studies in low-energy ion collisions with neutral complex systems.[8,23,24,42]

The position of avoided crossings in the perpendicular orientation of the colliding ion is similar to the case in which the THF molecule is in $C_s$ symmetry. This indicates that such a behaviour strongly depends on the orientation of the target molecule and that the collisional system is dominated by short range avoided crossings between the different potentials. In spite of important anisotropic effects, the mechanisms observed above can play a dominant role and may drive different dynamics in the $C^{2+}$–THF reaction.

### 3.3. Cross sections

The corresponding absolute averaged charge transfer cross section values in planar, close to planar (with deviation of the oxygen atom of about $\alpha = 23.34^\circ$ from the plane of the THF) and perpendicular ($\theta = 90^\circ$) orientations are presented in Table 1 and Fig. 7. The cross sections in the planar or near planar orientations are presented for both structures of THF in $C_{2v}$ and $C_s$ symmetry and calculated with inclusion of the potentials and corresponding couplings obtained with the CAS(10,8) active space. The perpendicular orientation is considered only for the $C_{2v}$ orientation of THF with the smaller CAS(6,6) active space in order to show the anisotropy of the

Table 1 Charge transfer cross sections for the $C^{2+}$–THF collisional system (in $10^{-16}$ cm$^2$)

| Velocity (a.u.) | $E_{lab}$ (eV) | $\sigma_{tot}$ ($C_{2v}$) plane | $\sigma_{tot}$ ($C_{2v}$) perp | $\sigma_{tot}$ ($C_s$) |
|---|---|---|---|---|
| 0.007 | 14.7 | $1.17 \times 10^{-7}$ | $1.2978 \times 10^{-5}$ | $7.1585 \times 10^{-3}$ |
| 0.01 | 30 | $3.86 \times 10^{-7}$ | $4.1663 \times 10^{-5}$ | $1.5116 \times 10^{-2}$ |
| 0.015 | 67.5 | $9.72 \times 10^{-7}$ | $8.5604 \times 10^{-5}$ | $2.7128 \times 10^{-2}$ |
| 0.02 | 120 | $1.08 \times 10^{-6}$ | $1.3159 \times 10^{-4}$ | $2.4096 \times 10^{-2}$ |
| 0.03 | 270 | $3.32 \times 10^{-6}$ | $1.3858 \times 10^{-4}$ | $3.9457 \times 10^{-2}$ |
| 0.04 | 480 | $2.84 \times 10^{-6}$ | $1.3099 \times 10^{-4}$ | 0.14629 |
| 0.05 | 750 | $2.19 \times 10^{-6}$ | $1.3057 \times 10^{-4}$ | 0.21793 |
| 0.06 | $1.08 \times 10^3$ | $3.31 \times 10^{-6}$ | $1.1848 \times 10^{-4}$ | 0.15035 |
| 0.07 | $1.47 \times 10^3$ | $4.41 \times 10^{-6}$ | $1.0966 \times 10^{-4}$ | 0.23922 |
| 0.1 | $3.0 \times 10^3$ | $2.94 \times 10^{-6}$ | $8.9648 \times 10^{-5}$ | 0.36644 |
| 0.15 | $6.75 \times 10^3$ | $3.19 \times 10^{-6}$ | $6.9418 \times 10^{-5}$ | 0.33747 |
| 0.2 | $12.0 \times 10^3$ | $3.08 \times 10^{-6}$ | $5.1324 \times 10^{-5}$ | 0.29235 |

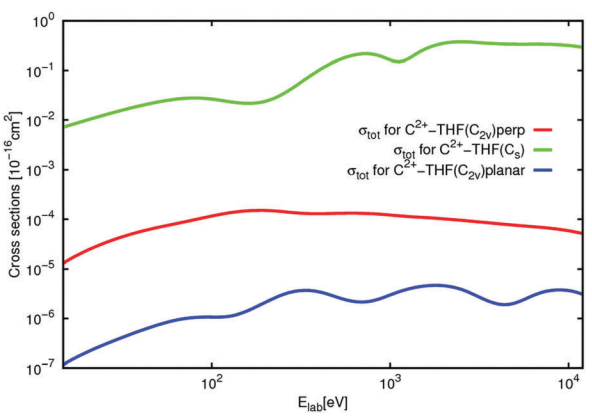


Fig. 7 Charge transfer cross sections in the $C^{2+}$–THF collision system: (blue), in-the-plane approach; (red), perpendicular approach; and (green), collision for THF in $C_s$ symmetry.

collision model. As the process is clearly anisotropic, such a model can provide a rough estimate of the accuracy of the cross sections with respect to the experimental conditions. However, the obtained absolute values for the charge transfer cross section can give only an order of magnitude of the process with regard to the limited number of states. In the following discussion, the obtained cross sections are interpreted starting from the lowest values and progressing to the highest.

Indeed, as can be seen in Fig. 7, the lowest values are obtained for the collision of $C^{2+}$ alongside the C–O bond in-the-plane of the tetrahydrofuran ($C_{2v}$, planar conformer) molecule for CAS(10,8). In this case, the $C^{2+}$–THF collision system shows clearly a regular increase in the charge transfer cross sections with increasing velocity, at low energies. The values of $\sigma_{tot}$ for the $C^{2+}$–THF ($C_{2v}$) planar reach a smooth maximum, around $3.32 \times 10^{-6} \times 10^{-16}$ cm$^2$ for $E_{lab}$ around 270 eV. Then, for higher energies they remain more or less constant with only small oscillating variations, around $[3.0–4.0] \times 10^{-6} \times 10^{-16}$ cm$^2$. The observed oscillatory dependence of the cross sections is due to interference between the energetically close reaction channels appearing as a result of interactions at large distances between the projectile and the target. This structure does not disappear after integration with respect to the impact parameter. Indeed, the oscillatory behaviour comes also from the existence of the avoided crossing of adiabatic potentials involved in the collision system and appears mostly in the lower collision energy region below 10 keV. Although within all energy ranges we observe a slow increase of the cross sections in this planar attack, the values always remain very small, reaching an order of magnitude of around $\times 10^{-22}$ cm$^2$. This can be explained by the lack of a significant avoided crossing region for the potential energy curves considered for such a collision (as illustrated in Fig. 4a and 5). Therefore, the likelihood of having an important charge transfer in this case is rather weak. Such a conclusion may be significant in relation to the experimental collisional data on the fragmentation processes.[20] The charge transfer process seems to be more efficient when the $C^{2+}$ ion is colliding with the THF target in the perpendicular orientation. This is particularly effective at very low eV impact energies, where the charge transfer cross sections are higher by about two orders of magnitude in the perpendicular attack rather than in the planar collision (Fig. 7, $\sigma_{tot}$ for $C^{2+}$–THF ($C_{2v}$) perp. and $\sigma_{tot}$ for $C^{2+}$–THF ($C_{2v}$) planar, respectively). The behaviour of the $C^{2+}$–THF ($C_s$ symmetry, envelope conformation) collision system appears to be quite different. Effectively, the cross section first continuously increases at very low energies (up to $\sim$400 eV), then shows a smooth minimum with small variations of charge transfer cross sections with velocity around $E_{lab}$ = 480 eV [$0.14629 \times 10^{-16}$ cm$^2$]. Besides, a strong increase of about one order of magnitude of the cross section values for energies up to 1 keV with evidence of a small minimum of around $0.15 \times 10^{-16}$ cm$^2$ is observed. For higher velocities, the values of charge transfer cross sections, $\sigma_{tot}$ for $C^{2+}$–THF ($C_s$), remain more or less constant, peaking around $0.36 \times 10^{-16}$ cm$^2$ in the range of energy between [3–12] keV. It is also clearly visible that all these values are at least two orders of magnitude greater than the ones observed for the $C^{2+}$–THF ($C_{2v}$) in perpendicular attack and up to $10^6$ higher compared to the planar attack.

For a more detailed assessment of the sensitivity of our results to the uncertainty of the cross sections, our results were compared with previous calculations performed for the $C^{4+}$ ion-induced collision with a 2-deoxy-D-ribose (dR) target in the furanose conformation.[36,60] In the backbone of DNA, the 2-deoxy-D-ribose sugar exists mainly in its furanose form, thus, tetrahydrofuran can be regarded as a simple analogue of the dR molecule. Calculations of the charge transfer cross sections for the $C^{4+}$–dR case have been performed in the [120 eV–108 keV] laboratory energy range in both restricted orientations, in the *xy* plane corresponding to the mean plane of the ring of the dR molecule, and in the perpendicular orientation along the *z* axis. The cross sections in perpendicular and planar orientations are displayed in Fig. 8, for both $C^{2+}$ and $C^{4+}$ projectile ions colliding with the THF and dR target molecules, respectively. Effectively, strong conformation and orientation dependence in carbon ion-induced collisions with both DNA building blocks may directly be observed. From the present results, it appears to be clear that for both collision systems, the charge transfer is favoured in the perpendicular or close to perpendicular geometry. In contrast, in the planar attack, the charge transfer process appears not to be particularly efficient.

However, the values of the cross sections for the $C^{2+}$–THF ($C_{2v}$ symmetry) collision system in-the-plane orientation are significantly lower than the charge transfer cross sections calculated also for $C^{4+}$–dR in-the-plane orientation, reaching at the maximum, an order of magnitude of $10^{-4} \times 10^{-16}$ cm$^2$. Such a result is not surprising since it was confirmed both by experimental data[61] and a series of calculations for collisions with carbon ions for $q > 2$,[22,62,63] that, generally, a higher charged projectile ion can induce higher charge transfer cross sections.

On the other hand, the low values of the cross sections can also be analyzed in relation to the experimental observations, considering that the relative fragmentation yield for a molecular

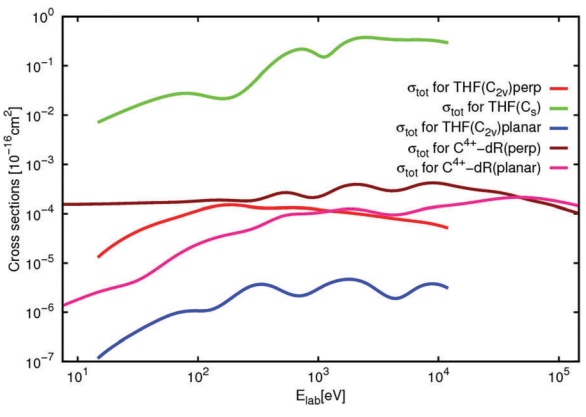


Fig. 8 Charge transfer cross sections for $C^{2+}$–THF (in the planar and perpendicular orientation, $C_{2v}$ symmetry of THF), $C^{2+}$–THF ($C_s$ symmetry) as well as for collision of the $C^{4+}$–dR sugar moiety in furanose form for the planar and perpendicular orientations. Color code: (blue), in-the-plane approach for $C^{2+}$–THF ($C_{2v}$); (red), perpendicular approach for $C^{2+}$–THF ($C_{2v}$); (green), collision for $C^{2+}$–THF ($C_s$ symmetry); (magenta), in-the-plane approach for $C^{4+}$–dR; and (brown), perpendicular orientation for $C^{4+}$–dR.

target after impact with a projectile ion can be assumed to be inversely proportional to the electron capture cross section.[4,61,64] Therefore, the obtained very low values of the cross sections in the planar attack for $C^{2+}$–THF can be regarded as evidence of efficient fragmentation of the molecular target during the collision. Indeed, such an assumption has been confirmed by experimental observations,[65] taking into account various projectiles for different collision energies. Moreover, our results show the importance of the assessment of the general features for the 5-membered DNA analogue and give the order of magnitude of the considered process.

## 4. Conclusions

In this work, we present a complete theoretical study of a fundamental charge transfer process occurring in collision between multiply charged carbon ions and biomolecules in the context of investigating radiation damage in biological systems. This study presents a model of the charge exchange interaction, considering the collision between $C^{2+}$ ions and THF in the frame of a molecular treatment of collision dynamics. A detailed theoretical analysis of the electronic structure of the target THF molecule by employing several very accurate quantum chemistry approaches has been shown in order to determine the geometry of the molecule and its excited states, and to define the most important orbitals, which were included in the chosen active spaces.

Different collision orientations have been considered taking into account two conformations of the target THF molecule (in planar $C_{2v}$ and envelope $C_s$ symmetry). Planar and perpendicular attacks of the $C^{2+}$ projectile on the THF target were investigated using *ab initio* potential energy curves and couplings calculated along internuclear distance $R$ followed by a semiclassical collisional treatment in the impact energy range from eV to keV. In order to identify single and double electron capture channels, particularly special attention has been paid to the exploration of the adiabatic potential energy curves. Strong delocalization of the $\pi$ electrons of the THF ring towards the $C^{2+}$ ion, leading to the creation of a chemical bond between the oxygen atom and the colliding ion, has been observed. The presence of the cluster $[C^+–C_4H_8O]^+$ temporarily formed during the interaction has been noticed, which confirms the experimental prediction[20] for the $C^+$–THF system. Another important finding of this work concerns the calculated values of charge transfer cross sections, which strongly depend on the orientation of the THF molecule considered in the collision framework. Despite the smaller active space used for the calculation, it appears to be clear that the perpendicular attack is preferable to the planar attack for impacting electron transfer. Differences in cross section values are mainly caused by two variables: (i) the existence of the two important avoided crossing regions and strong degeneration of the states at the long range observed for the perpendicular orientation in the molecular structure calculations and (ii) strong anisotropy of the symmetry of the THF molecule from $C_{2v}$ to $C_s$ displacement of the $\alpha$ angle. It has been pointed out that a change in the THF symmetry from $C_{2v}$ to $C_s$ during collision with $C^{2+}$ ions leads to a significant increase in the cross section values up to three orders of magnitude. Taking into account the dependence between the fragmentation and electron capture processes, this would suggest that the charge transfer process seems to be the most efficient and is playing the most significant role when the carbon ion is colliding with the tetrahydrofuran target in $C_s$ symmetry with displaced orientation along the C5–O1 bond. From the present results, it appears that the consideration of the $n_O(2p_z^O)$ orbital centered on the oxygen of the THF molecule is absolutely necessary in order to provide an adequate determination of the charge transfer cross sections. This feature is in agreement with the previous calculations of M.-C. Bacchus-Montabonel for $C^{4+}$ ions interacting with the 2-deoxy-D-ribose molecule, where delocalization between two $2p_z$ orbitals situated on the oxygen atoms taking part in the molecular model was observed.[35] The low values of the calculated charge transfer cross sections would also suggest almost complete decay of 2-deoxy-D-ribose and its simple analogue (especially in its $C_{2v}$ structure) in ion-induced collisions.

Therefore, to analyze further the influence of the orientation of the target molecule of biological meaning in collision with carbon ions, additional calculations, including all the conformers of THF as well as different heterocyclic molecules, should be performed. The influence of the charge state of the carbon ions should also be investigated. This will certainly allow us to understand in detail the anisotropy of electron capture processes in ion-induced collisions with DNA sugar analogues, especially in relation to new experimental findings.[66] Particularly, it has been suggested that collisions with carbon ions lead to a more efficient dissociation of THF than collisions with protons. Therefore, looking deeply into the context of the role and efficiency of the charge transfer processes in cancer proton therapy, the model collisions of protons with bio(molecular) targets should also be investigated theoretically. Additionally, since a complete approach should also take into account the fragmentation processes, presently we are investigating the decomposition of the simpler furan molecule by means of different state of the art quantum chemistry approaches.

The present work thus can be regarded as a background to the study of the fragmentation processes induced by the collision of ions and protons with biologically relevant molecules or their five- and six-membered heterocyclic analogues, which we hope to present in the near future. A complete approach should take into account forthcoming experimental fragmentation measurements of the THF molecule by ion impact. The obtained experience and results might then be used as a basis to extend the theoretical studies to other RNA or DNA bases in a real environment, such as aqueous solution.

## Acknowledgements

We gratefully acknowledge financial support from COST Action CM1204 (XLIC) and Gdańsk University of Technology. The molecular calculations were performed at the Academic Computer Centre in Gdańsk (CI TASK) and the Wroclaw Centre for

Networking and Supercomputing, grant No. 383. M. Łabuda and M.-C. Bacchus-Montabonel acknowledge support from the computer center CCIN2P3 in Lyon and HPC resources of CCRT/CINES/IDRIS under the allocation made by Grand Equipement National de Calcul Intensif (GENCI).

## References


1 B. D. Michael and P. D. O'Neill, *Science*, 2000, **287**, 1603.
2 B. Boudaïffa, P. Cloutier, D. Hunting, M. A. Huels and L. Sanche, *Science*, 2000, **287**, 1658.
3 G. Vall-Llosera, M. A. Huels, M. Coreno, A. Kivimäki, K. Jakubowska, M. Stankiewicz and E. Rachlew, *ChemPhysChem*, 2008, **9**, 1020.
4 O. González-Magaña, M. Tiemens, G. Reitsma, L. Boschman, M. Door, S. Bari, P. O. Lahaie, J. R. Wagner, M. A. Huels, R. Hoekstra and T. Schlathölter, *Phys. Rev. A: At., Mol., Opt. Phys.*, 2013, **87**, 1.
5 F. Gianturco and R. R. Lucchese, *J. Chem. Phys.*, 2004, **120**, 7446.
6 Z. Deng, M. Imhoff and M. A. Huels, *J. Chem. Phys.*, 2005, **123**, 144509.
7 L. Sanche, *Eur. Phys. J. D*, 2005, **35**, 367.
8 J. De Vries, R. Hoekstra, R. Morgenstern and T. Schlathölter, *Eur. Phys. J. D*, 2003, **24**, 161.
9 J. De Vries, R. Hoekstra, R. Morgenstern and T. Schlathölter, *J. Phys. B: At., Mol. Opt. Phys.*, 2002, **35**, 21.
10 T. Schlathölter, R. Hoekstra and R. Morgenstern, *Int. J. Mass Spectrom.*, 2004, **233**, 1.
11 T. J. Wasowicz, A. Kivimäki, M. Dampc, M. Coreno, M. De Simone and M. Zubek, *Phys. Rev. A: At., Mol., Opt. Phys.*, 2011, **83**, 033411.
12 P. M. Mayer, M. F. Guest, L. Cooper, L. G. Shpinkova, E. E. Rennie, D. M. P. Holland and D. A. Shaw, *J. Phys. Chem. A*, 2009, **113**, 10923.
13 M. Dampc, E. Szymanska, B. Mielewska and M. Zubek, *J. Phys. B: At., Mol. Opt. Phys.*, 2011, **44**, 055206.
14 T. P. T. Do, M. Leung, M. Fuss, G. Garcia, F. Blanco, K. Ratnavelu and M. J. Brunger, *J. Chem. Phys.*, 2011, **134**, 1.
15 P. Mozejko, E. Ptasińska-Denga, A. Domaracka and C. Szmytkowski, *Phys. Rev. A: At., Mol., Opt. Phys.*, 2006, **74**, 12708.
16 C. J. Colyer, S. M. Bellm, B. Lohmann, G. F. Hanne, O. Al-Hagan, D. H. Madison and C. G. Ning, *J. Chem. Phys.*, 2010, **133**, 124302.
17 M. C. Fuss, R. Colmenares, A. G. Sanz, A. Muñoz, J. C. Oller, F. Blanco, T. P. T. Do, M. J. Brunger, D. Almeida, P. Limão-Vieira and G. García, *J. Phys.: Conf. Ser.*, 2012, **373**, 12010.
18 D. Almeida, F. Ferreira da Silva, S. Eden, G. Garcia and P. Limão-Vieira, *J. Phys. Chem. A*, 2014, **118**, 690.
19 D. Almeida, F. Ferreira da Silva, G. Garcia and P. Limão-Vieira, *J. Chem. Phys.*, 2013, **139**, 114304.
20 T. J. Wasowicz and B. Pranszke, *J. Phys. Chem. A*, 2015, **119**, 581.
21 M. C. Bacchus-Montabonel, M. Łabuda, Y. S. Tergiman and J. E. Sienkiewicz, *Phys. Rev. A: At., Mol., Opt. Phys.*, 2005, **72**, 052706.
22 M. C. Bacchus-Montabonel, *Eur. Phys. J. D*, 2012, **66**, 175/7.
23 M. C. Bacchus-Montabonel, *Appl. Radiat. Isot.*, 2014, **83**, 95.
24 M. C. Bacchus-Montabonel and Y. S. Tergiman, *Phys. Rev. A: At., Mol., Opt. Phys.*, 2006, **74**, 054702/4.
25 P. Sulzer, S. Ptasinska, F. Zappa, B. Mielewska, A. R. Milosavljevic, P. Scheier, T. D. Märk, I. Bald, S. Gohlke, M. A. Huels and E. Illenberger, *J. Chem. Phys.*, 2006, **125**, 044304.
26 S.-H. Lee, *Phys. Chem. Chem. Phys.*, 2010, **12**, 2655.
27 A. Lifshitz, M. Bidani and S. Bidani, *J. Phys. Chem.*, 1986, **90**, 3422.
28 D. G. Melnik, S. Gopalakrishnan, T. A. Miller and F. C. De Lucia, *J. Chem. Phys.*, 2003, **118**, 3589.
29 V. M. Rayón and J. A. Sordo, *J. Chem. Phys.*, 2005, **122**, 204303.
30 A. Giuliani, P. Limão-Vieira, D. Duflot, A. R. Milosavljevic, B. P. Marinkovic, S. V. Hoffmann, N. Mason, J. Delwiche and M. J. Hubin-Franskin, *Eur. Phys. J. D*, 2009, **51**, 97.
31 B. Cadioli, E. Gallinella, C. Coulombeau, H. Jobic and G. Berthier, *J. Phys. Chem.*, 1993, **97**, 7844.
32 P. K. Sahu, A. Chaudhari and S. L. Lee, *Chem. Phys. Lett.*, 2004, **386**, 351.
33 E. Erdmann and M. Łabuda, *J. Phys.: Conf. Ser.*, 2015, **635**, 22097.
34 M. A. Hervé du Penhoat, P. López-Tarifa, K. K. Ghose, Y. Jeanvoine, M. P. Gaigeot, R. Vuilleumier, M. F. Politis and M. C. Bacchus-Montabonel, *J. Mol. Model.*, 2014, **20**, 2221.
35 M. C. Bacchus-Montabonel, *J. Phys. Chem. A*, 2014, **118**, 6326.
36 M. C. Bacchus-Montabonel, *J. Phys. Chem. A*, 2013, **117**, 14169.
37 M. Łabuda, Y. S. Tergiman, M. C. Bacchus-Montabonel and J. E. Sienkiewicz, *Chem. Phys. Lett.*, 2004, **394**, 446.
38 M. Łabuda, Y. S. Tergiman, M. C. Bacchus-Montabonel and J. E. Sienkiewicz, *Int. J. Mol. Sci.*, 2004, **5**, 265.
39 M. C. Bacchus-Montabonel, *Phys. Rev. A: At., Mol., Opt. Phys.*, 1999, **59**, 3569.
40 M. C. Bacchus-Montabonel, M. Łabuda, Y. S. Tergiman and J. E. Sienkiewicz, *Progress in Theoretical Chemistry and Physcis*, Springer, College. Park. Md., 2007, vol. 16, p. 203.
41 E. Bene, P. Martínez, G. J. Halász, Á. Vibók and M. C. Bacchus-Montabonel, *Phys. Rev. A: At., Mol., Opt. Phys.*, 2009, **80**, 012711.
42 M. C. Bacchus-Montabonel and Y. S. Tergiman, *Chem. Phys. Lett.*, 2011, **503**, 45.
43 N. Vaeck, M. Desouter-Lecomte and J. Liévin, *J. Phys. B: At., Mol. Opt. Phys.*, 1999, **32**, 409.
44 N. Vaeck, M. C. Bacchus-Montabonel, E. Baloïtcha and M. Desouter-Lecomte, *Phys. Rev. A: At., Mol., Opt. Phys.*, 2001, **63**, 427041.
45 E. Baloïtcha, M. Desouter-Lecomte, M. C. Bacchus-Montabonel and N. Vaeck, *J. Chem. Phys.*, 2001, **114**, 8741.
46 M. Łabuda, J. González-Vázquez and L. González, *Phys. Chem. Chem. Phys.*, 2010, **12**, 5439.
47 M. Łabuda, J. González-Vázquez, F. Martín and L. González, *Chem. Phys.*, 2012, **400**, 165.
48 A. Chenel, E. Mangaud, Y. Justum, D. Talbi, M. C. Bacchus-Montabonel and M. Desouter-Lecomte, *J. Phys. B: At., Mol. Opt. Phys.*, 2010, **43**, 245701.
49 R. J. Allan, C. Courbin, P. Salas and P. Wahnon, *J. Phys. B: At., Mol. Opt. Phys.*, 1990, **23**, L461.

50 H.-J. Werner, P. J. Knowles, G. Knizia, F. R. Manby and M. Schütz, *Wiley Interdiscip. Rev.: Comput. Mol. Sci.*, 2012, **2**, 242.
51 H.-J. Werner, P. J. Knowles, G. Knizia, F. R. Manby, M. Schütz, P. Celani, W. Györffy, D. Kats, T. Korona, R. Lindh, A. Mitrushenkov, G. Rauhut, K. R. Shamasundar, T. B. Adler, R. D. Amos, A. Bernhardsson, A. Berning, D. L. Cooper, M. J. O. Deegan, A. J. Dobbyn, F. Eckert, E. Goll, C. Hampel, A. Hesselmann, G. Hetzer, T. Hrenar, G. Jansen, C. Köppl, Y. Liu, A. W. Lloyd, R. A. Mata, A. J. May, S. J. McNicholas, W. Meyer, M. E. Mura, A. Nicklass, D. P. O'Neill, P. Palmieri, D. Peng, K. Pflüger, R. Pitzer, M. Reiher, T. Shiozaki, H. Stoll, A. J. Stone, R. Tarroni, T. Thorsteinsson and M. Wang, MOLPRO ver.2015.1, 2015.
52 A. D. Becke, *Phys. Rev. A: At., Mol., Opt. Phys.*, 1988, **38**, 3098.
53 A. D. Becke, *J. Chem. Phys.*, 1993, **98**, 5648.
54 C. Lee, W. Yang and R. G. Parr, *Phys. Rev. B: Condens. Matter Mater. Phys.*, 1988, **37**, 785.
55 J. F. Stanton and R. J. Bartlett, *J. Chem. Phys.*, 1993, **98**, 7029.
56 B. O. Roos, *Ab initio methods in Quantum Chemistry II*, Wiley-VCH, Chichester, 1987, pp. 399–445.
57 T. Schlathölter, F. Alvarado, S. Bari and R. Hoekstra, *Phys. Scr.*, 2006, **73**, C113.
58 F. Alvarado, S. Bari, R. Hoekstra and T. Schlathölter, *J. Chem. Phys.*, 2007, **127**, 034301.
59 S. Maclot, M. Capron, R. Maisonny, A. Lawicki, A. Mery, J. Rangama, J.-Y. Chesnel, S. Bari, R. Hoekstra and T. Schlathölter, *ChemPhysChem*, 2011, **12**, 930.
60 M. C. Bacchus-Montabonel, *Eur. Phys. J. D*, 2015, **69**, 107.
61 A. N. Agnihotri, S. Kasthurirangan, S. Nandi, A. Kumar, M. E. Galassi, R. D. Rivarola, O. Fojon, C. Champion, J. Hanssen, H. Lekadir, P. F. Weck and L. C. Tribedi, *Phys. Rev. A: At., Mol., Opt. Phys.*, 2012, **85**, 1.
62 C. Illescas, L. F. Errea and L. Méndez, *Phys. Scr.*, 2013, **T156**, 14033.
63 M. C. Bacchus-Montabonel, Y. S. Tergiman and D. Talbi, *Phys. Rev. A: At., Mol., Opt. Phys.*, 2009, **79**, 012710.
64 F. Alvarado, S. Bari, R. Hoekstra and T. Schlathölter, *Phys. Chem. Chem. Phys.*, 2006, **8**, 1922.
65 Z. Deng, I. Bald, E. Illenberger and M. A. Huels, *Phys. Rev. Lett.*, 2005, **95**, 153201.
66 T. J. Wasowicz and B. Pranszke, *Eur. Phys. J. D*, 2016, **70**, 175.